Molecular Systems Biology 9; Article number 657; doi:10.1038/msb.2013.17
Citation: ***Molecular Systems Biology*** **9:657**
www.molecularsystemsbiology.com

OPEN ACCESS TRANSPARENT PROCESS

molecular systems biology

Global remodelling of cellular microenvironment due to loss of collagen VII

Victoria Küttner[1,2,3,4], Claudia Mack[3], Kristoffer TG Rigbolt[1,2], Johannes S Kern[3], Oliver Schilling[5,6], Hauke Busch[1,2,5], Leena Bruckner-Tuderman[1,2,3,6,*] and Jörn Dengjel[1,2,6,*]

[1] School of Life Science-LifeNet, Freiburg Institute for Advanced Studies (FRIAS), University of Freiburg, Freiburg, Germany, [2] ZBSA Center for Biological Systems Analysis, University of Freiburg, Freiburg, Germany, [3] Department of Dermatology, University Freiburg Medical Center, Freiburg, Germany, [4] Faculty of Biology, University of Freiburg, Freiburg, Germany, [5] Institute for Molecular Medicine and Cell Research, University of Freiburg, Freiburg, Germany and [6] BIOSS Centre for Biological Signalling Studies, University of Freiburg, Freiburg, Germany
* Corresponding authors. L Bruckner-Tuderman or J Dengjel, School of Life Science-LifeNet, Freiburg Institute for Advanced Studies (FRIAS), University of Freiburg, Albertstrasse 19, Freiburg 79104, Germany. Tel.: + 49 761 270 67160; Fax: + 49 761 270 69360; E-mail: bruckner-tuderman@uniklinik-freiburg.de or Tel.: + 49 761 203 97208; Fax: + 49 761 203 97241; joern.dengjel@frias.uni-freiburg.de

Received 6.12.12; accepted 13.3.13

The mammalian cellular microenvironment is shaped by soluble factors and structural components, the extracellular matrix, providing physical support, regulating adhesion and signalling. A global, quantitative mass spectrometry strategy, combined with bioinformatics data processing, was developed to assess proteome differences in the microenvironment of primary human fibroblasts. We studied secreted proteins of fibroblasts from normal and pathologically altered skin and their post-translational modifications. The influence of collagen VII, an important structural component, which is lost in genetic skin fragility, was used as model. Loss of collagen VII had a global impact on the cellular microenvironment and was associated with proteome alterations highly relevant for disease pathogenesis including decrease in basement membrane components, increase in dermal matrix proteins, TGF-β and metalloproteases, but not higher protease activity. The definition of the proteome of fibroblast microenvironment and its plasticity in health and disease identified novel disease mechanisms and potential targets of intervention.

Molecular Systems Biology **9:** 657 published online 16 April 2013; doi:10.1038/msb.2013.17
Subject Categories: proteomics; molecular biology of disease
Keywords: disease proteomics; extracellular matrix (ECM); mass spectrometry; MMP14; primary human fibroblasts

Introduction

Mammalian cells secrete soluble and structural proteins into the extracellular space. The structural components make up the extracellular matrix (ECM) and both, matrix and soluble proteins, such as growth factors, proteases and cytokines, shape the cellular microenvironment and regulate cell functions. Transmembrane receptors like integrins connect the extracellular space with intracellular signal transduction relays. The ECM regulates not only cell adhesion, but also bioavailability of growth factors and composition of membrane receptors (Brizzi *et al*, 2012). The human skin consists of an epithelium, the epidermis and a subjacent mesenchymal tissue, the dermis, which both generate complex and functionally specialised ECMs: the subepidermal basement membrane and dermal networks of fibrillar collagens and associated proteins. Cell–ECM interactions in the skin have a vital role in tissue homeostasis, wound healing and ageing, and are often deregulated in disease (Watt and Fujiwara, 2011). Hence, its importance and its easy accessibility make skin ECM highly attractive for studying ECM composition and plasticity.

Physiological skin integrity and resistance to mechanical stress rely on the functions of the dermal-epidermal junction zone (DEJZ), which anchors the epidermis to the underlying dermis. Protein complexes at the DEJZ, such as hemidesmosomes and focal adhesion complexes, mediate interactions of the cytoskeleton in basal keratinocytes with the basement membrane. Anchoring fibrils, which emanate from the basement membrane into the dermis and entrap dermal collagen bundles, establish stable dermal-epidermal adhesion. The major component of the anchoring fibrils is collagen VII (C7) (Has and Bruckner-Tuderman, 2006).

Loss of C7 causes recessive dystrophic epidermolysis bullosa (RDEB), an inherited monogenic skin disorder with diminished dermal-epidermal adhesion, mechanically induced skin blistering and subsequent scarring (Fine *et al*, 2008). Mutations in the C7 gene, *COL7A1*, are associated with a broad range of clinical phenotypes, ranging from localised manifestations to generalised mucocutaneous blistering and scarring, and to high risk of aggressive skin cancer (Kern *et al*, 2006; van den Akker *et al*, 2011). Genotype–phenotype correlation studies on RDEB have shown that null mutations

© 2013 EMBO and Macmillan Publishers Limited

and absence of C7 are associated with severe RDEB, whereas hypomorphic mutations cause milder RDEB forms (Hammami-Hauasli *et al*, 1998). Intriguingly, there are significant interindividual differences in patients with identical *COL7A1* mutations (Kern *et al*, 2009).

Very little information exists on the consequences of loss of C7 at the cellular level and in relation to the cellular microenvironment. Loss of the structural function of C7 perturbs its interaction with laminin-332, which provides dermal-epidermal anchorage and is also required for keratinocyte survival (Waterman *et al*, 2007). *In vivo,* C7 deficiency was associated with increased TGF-β1 and accumulation of dermal ECM proteins in skin (Fritsch *et al*, 2008). In three-dimensional cultures *in vitro*, C7-deficient keratinocytes became invasive, and recent studies suggested that RDEB fibroblast ECM, like cancer-associated fibroblast ECM, drives development of cutaneous squamous cell carcinoma (Martins *et al*, 2009; Ng *et al*, 2012). Additionally, differences in collagen breakdown by matrix metalloproteases (MMPs) may contribute to distinct RDEB phenotypes (Titeux *et al*, 2008).

Proteomic analysis using mass spectrometry (MS) represents a state-of-the-art unbiased and global approach (Zimmermann *et al*, 2010; Engelke *et al*, 2012) to questions relating to disease pathogenesis. Few studies have investigated secreted proteins of skin cells, including human dermal fibroblasts, mouse keratinocytes and human oral squamous cell carcinoma lines (Boraldi *et al*, 2003; Pflieger *et al*, 2006; Del Galdo *et al*, 2010; Todorovic *et al*, 2010), but the analyses were mainly of qualitative nature and the number of identified proteins low. In a recent systems biology study, the role of MMP2 in skin inflammation was investigated by employing isobaric tags for relative and absolute quantitation (iTRAQ) highlighting the power of global quantitative proteomics (auf dem Keller *et al*, 2013). Here, we developed a comprehensive approach by employing stable isotope labelling by amino acids in cell culture (SILAC)-based quantitative MS (Ong *et al*, 2002), followed by bioinformatics analyses, to investigate quantitative differences of secreted proteins and respective post-translational modifications (PTMs) in human dermal fibroblasts derived from normal and pathologically altered skin, C7-negative RDEB being our model system. We identified and quantified patient-specific and general alterations of the extracellular proteome upon C7 loss and generated an atlas of oxidative PTMs important for structural stability, providing a valuable resource of proteins shaping the cellular microenvironment. Hitherto unknown proteins, molecular pathways and mechanisms involved in RDEB pathogenesis were identified.

Results

Secretome of normal skin fibroblasts

For proteomic profiling of proteins secreted by primary human skin fibroblasts, cells were processed as shown in Figure 1A. Secreted proteins were divided into two fractions: (a) cell conditioned medium (CM) comprising all soluble proteins and (b) insoluble proteins remaining on the culture plate after cell lysis. The latter was defined as ECM in the experimental setting used here. The CM was harvested at day 4, and the ECM was purified at day 6 by removing the cells with basic Triton-NH_4OH (Vlodavsky, 2001), followed by protein extraction with 4% SDS. Compared with other isolation procedures this approach yielded the best results, i.e., a fibrillar matrix visible in the light microscope after cellular detachment, and enrichment of extracellular proteins, as judged by the respective GO (Supplementary Figure S1). The efficiency and purity of the ECM was confirmed by western blot (Figure 1B).

To globally characterise the composition of the fibroblast secretome, the proteins in the ECM and CM were fractionated by SDS–PAGE, in-gel digested with trypsin and analysed by LC-MS/MS, resulting in the identification of almost 2000 proteins with a false discovery rate (FDR) below 1%. Since the sensitivity of modern mass spectrometers is extremely high, it is likely that small amounts of contaminating intracellular proteins would be detected in the biochemically enriched fraction of extracellular proteins. To distinguish these and to generate a comprehensive list of ECM proteins, we employed a bioinformatics data processing pipeline using the following parameters (Figure 1C): (1) proteins carrying GO terms 'extracellular' (extracellular region, space and matrix) were filtered; (2) to identify new ECM components, all proteins reproducibly identified in the ECM and the CM were also considered as extracellular; (3) proteins predicted by *in silico* analysis to carry a signal peptide (SignalP; www.cbs.dtu.dk/services/SignalP/) (Petersen *et al*, 2011) were counted as extracellular (Henningsen *et al*, 2010). These measures yielded ∼660 extracellular proteins in the ECM and 740 in the CM from the total list of identified proteins, with >60% being detected in both fractions (Figure 1C). The filtered proteins were analysed based on their Swiss-Prot (SP) and Protein Information Resource (PIR) keywords (Figure 1D). While membrane proteins were enriched in the ECM fraction, proteins with enzymatic activities, such as proteases and hydrolases, were enriched in the CM, indicating the different nature of the two compartments. As expected, the terms secreted, ECM, and signal peptide, among others, were common to both groups.

To assess potential differences in the abundance of extracellular proteins in a physiological setting, we SILAC labelled skin fibroblasts of three healthy donors (Sprenger *et al*, 2010). CM and ECM were purified and the data processed as outlined above. In two biological replicates of ECM and CM, respectively, we quantified 863 potential extracellular proteins, of which 40% were annotated as being extracellular based on GO terms. We observed only minor donor-specific differences in ECM and CM, indicating that three samples were sufficient to capture proteome alterations in the used experimental settings (Figure 1E; Supplementary Tables S1 and S2). In all, 95% of proteins were in the interval of ± 0.75 (log2 SILAC ratios), not showing altered abundance in the different samples, and biological replicates showed good reproducibility ($r = 0.6–0.93$; Supplementary Figures S2 and S3). Thus, we established an experimental platform for global analysis of protein abundance differences of extracellular proteins, ECM and CM, and showed that extracellular proteins of primary skin fibroblasts of

© 2013 EMBO and Macmillan Publishers Limited

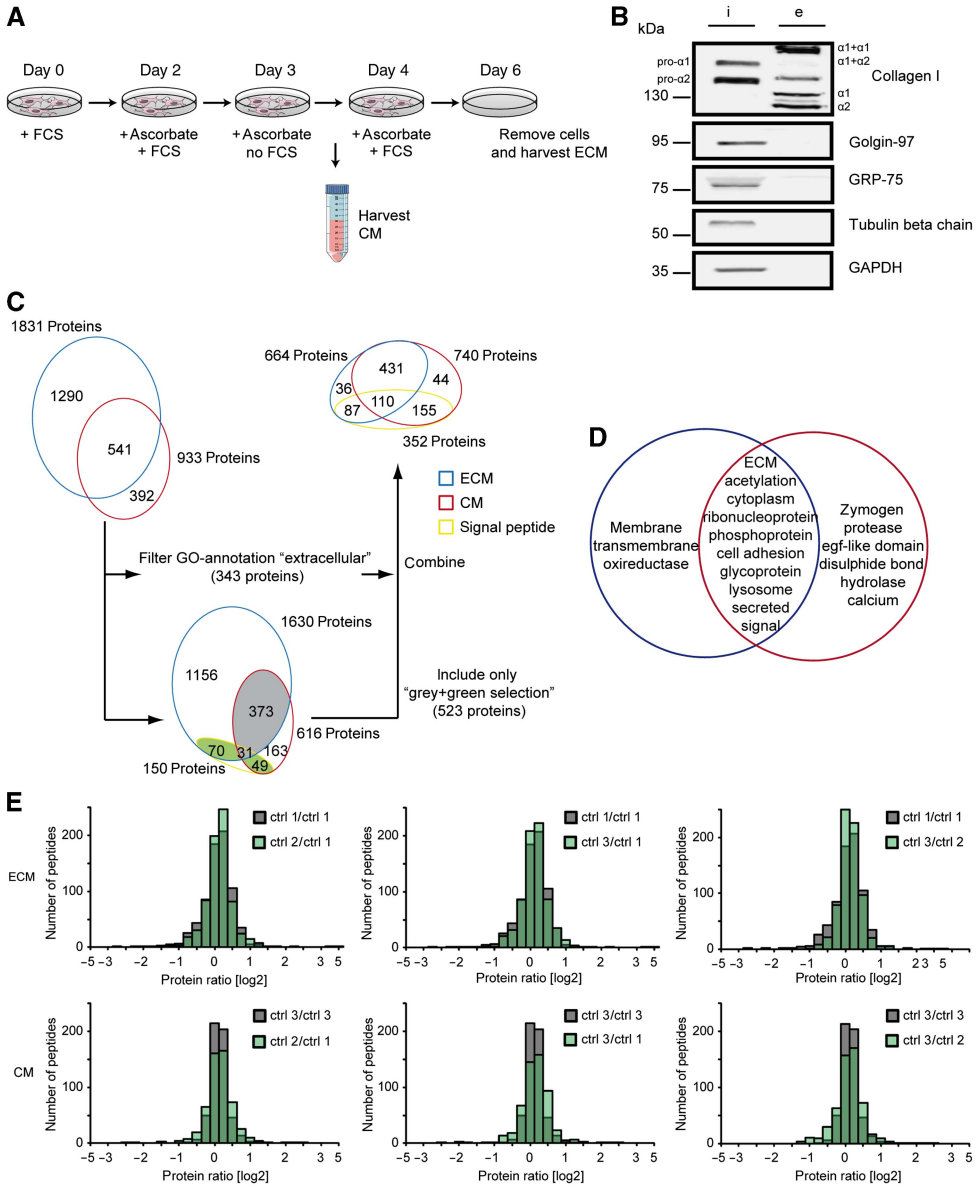

Figure 1 Experimental design and data processing pipeline. (**A**) Primary skin fibroblasts were kept in culture for 6 days. At days 2, 3, and 4, fresh culture medium containing ascorbate was added. The CM was harvested at day 4 and the ECM at day 6. (**B**) Intracellular proteins representing the cell compartments cytosol (Tubulin β chain, GAPDH), mitochondrion (GRP-75) and golgi apparatus (golgin-97) are only detected in the cell lysate (i). Procollagen I was in the cell lysate, whereas mature collagen I was found only in the ECM (e). (**C**) The ECM and CM were analysed by MS-based proteomics, and secreted proteins were filtered on (I) GO annotation 'extracellular', (II) proteins that were repeatedly detected in the ECM and the CM, and (III) proteins detected only in the ECM or the CM if they were predicted to have signal peptides. (**D**) SP and PIR keywords were used to highlight enriched protein classes (BH-adjusted *P*-value <0.05). (**E**) Experimental variability was analysed by quantitatively comparing protein abundances of differentially SILAC-labelled ECM and CM from the same donor (ctrl 1 and ctrl 3 in grey, respectively). Biological variability was analysed by comparing protein abundances of the ECM and the CM from different donors (in green). Figures were produced using Servier Medical Art (www.servier.com).

healthy donors exhibit only minor differences in their secretion pattern.

Interindividual variance of secreted proteins in fibroblasts upon loss of C7

To study the effects of loss of C7 on the composition of the secretome, skin fibroblasts of four individuals with RDEB and three healthy donors were SILAC labelled, subcultured to the same number of passages and subjected to the quantitative proteome analysis as described above. The diagnosis of RDEB was established by two criteria: complete lack of C7 in the skin and *COL7A1* mutations leading to a premature stop codon (Supplementary Figure S4; Table I). The ECMs of the three controls were combined to generate a Super-SILAC mix, minimising the interindividual influences of the healthy donors (Geiger *et al*, 2010). This mix was then spiked in equal

© 2013 EMBO and Macmillan Publishers Limited

Table I Characteristics of RDEB patients in this study

Patient	Age at biopsy (days)/ gender	Sampling location	*COL7A1* mutation	Consequence	Reference
1.	4/f	Thigh	425A>G 682+1 G>A	PTC PTC	Kern *et al* (2009)
2.	36/m	Thigh	425A>G c.5261dup	PTC p.G1755RfsX17	Kern *et al* (2009)
3.	6/f	Undisclosed	1732C>T 1732C>T	R578X R578X	Kern *et al* (2006)
4.	8/m	Undisclosed	c1934del c1934del	p.P645QfsX45 p.P645QfsX45	Kern *et al* (2009)

amounts into the ECMs purified from medium and heavy labelled RDEB cells (Figure 2A). Furthermore, Super-SILAC samples were also generated of ECMs labelled control cells using the same procedure as for the patients. Subsequently, samples and data were processed as outlined (Figures 2A, B and 1C). The same workflow was performed for the CM. Since the Super-SILAC mix was used as a common standard, it was possible to directly compare quantitative differences between the four RDEB and the three control samples. We quantified 587 potential extracellular proteins (45% carrying 'extracellular' GO terms) in a total set of 190 LC-MS/MS analyses comprising at least two biological replicates for all conditions (Supplementary Tables S3 and S4; Supplementary Figures S5 and S6). Of these, 154 proteins were identified only in CM samples (Supplementary Table S4). On average, 45.7% of the ECM proteins and 31.7% of the CM proteins of RDEB fibroblasts showed abundance differences larger than 0.75 (log2 SILAC ratio), much larger proportions than the 5% observed for the control fibroblasts.

As all four RDEB patients carried null mutations in the *COL7A1* gene, the question was raised whether the ECMs of RDEB fibroblasts generally show the same trend of alterations in their proteomic composition. To address this, we compared protein abundance differences by performing a principal component analysis (Figure 2C). Control and RDEB samples clearly separated, indicating general alterations in ECM composition in RDEB. However, it became evident that RDEB ECMs were more heterogeneous than control ECMs and showed patient-specific effects.

Modulated basement membrane and ECM proteomes in RDEB

Quantitative differences of secreted proteins in C7-deficient RDEB fibroblasts were analysed by hierarchical clustering of ECM (Figure 2D) and CM data (Supplementary Figure S7A). Generally, proteins carrying GO terms 'extracellular structure' and 'matrix organisation' were enriched in RDEB ECMs, whereas proteins related to 'cell morphogenesis' and 'cytoskeleton organisation' were less abundant. We examined proteins carrying the GO terms 'cell adhesion' and 'extracellular structure and organisation' in detail. For example, the interstitial collagens were increased in the ECMs of patients 1, 3 and 4. In contrast, in samples of patient 2, the polypeptides encoded by *COL1A1, COL1A2, COL3A1, COL5A1, COL5A2, COL12A1* and *COL15A1* did not accumulate. Also the collagen modifying enzymes lysyl oxidase homologs 1, 2, and lysyl hydroxylase 1, as well as the elastin microfibril interface-located proteins 1 and 2, were less abundant in the samples of patient 2 as compared with the other three patients (Supplementary Figure S8). The complete data sets demonstrating patient-specific differences are presented in Supplementary Tables S3 and S4.

Clustering of protein abundances in CM was in agreement with ECM findings separating RDEB and control samples (Supplementary Figure S7A). However, generally, the ECM values spread more than the CM values, and the respective data sets correlated only weakly ($r=0.25$). This could reflect altered protein–protein interactions and integration of individual proteins into the ECM suprastructures in RDEB samples (Supplementary Figure S7B). Highly abundant proteins in RDEB CM were TGF-β1, and the TGF-β-induced protein ig-h3.

Quantitative proteomics-based findings were validated with several methods. Western blot analyses of RDEB ECMs revealed less deposition of basement membrane proteins laminin β1, laminin γ1, nidogen 1 and fibulin 1, whereas tenascin C and TGF-β1-induced protein ig-h3 were accumulated (Figure 3A). These differences correlated well with SILAC MS ratios ($r=0.83$; Figure 3B). Also immunofluorescence stainings of ECM were in agreement with proteomics data (Figure 3C; Supplementary Figure S9C). Interestingly, laminin β1 and nidogen 1 were less abundant in ECMs but not in respective RDEB cell lysates, suggesting altered protein trafficking/ECM integration (Figure 3A and C; Supplementary Figure S9A–C). The corresponding *in vivo* data were congruent with the *in vitro* results. Immunofluorescence staining showed increased tenascin C and decreased collagen IV and laminin β1/γ1 deposition at the DEJZ in RDEB skin (Figure 3D). Paraffin-embedded specimens of normal and RDEB skin were assessed regarding the pattern and the intensity of Elastica van Gieson staining of the dermis. In control skin, the dermal ECM presented with a loose, undulating fibrillar network, incorporating regular interconnected elastic fibres (Figure 3E). In RDEB skin, the ECM was tightly packed, and the fibre orientation paralleled the skin surface, indicating quantitative increase in ECM proteins, as detected by the proteomics approach, and perturbed organisation, as seen in fibrosis. Quantitation of the normalised mean dermal staining intensity revealed a significant fibrotic change in RDEB dermis, as compared with localisation and age-matched control dermis.

To test whether the differences in protein abundance were directly linked to loss of C7, siRNA was used to knock down C7 in normal primary skin fibroblasts. This resulted in a decrease in laminin γ1 and an increase in collagen I in respective cell lysates as compared with controls and in agreement with proteomics findings (Supplementary Figure S9D and E; Supplementary Table S3).

Finally, linear models for microarray data (LIMMA) (Smyth, 2004) were used to identify consistent changes in ECM compositions between all RDEB and control fibroblasts and identified 214 proteins as significantly altered in all RDEB ECMs ($P<0.05$, BH adjusted; Supplementary Table S3). We

© 2013 EMBO and Macmillan Publishers Limited

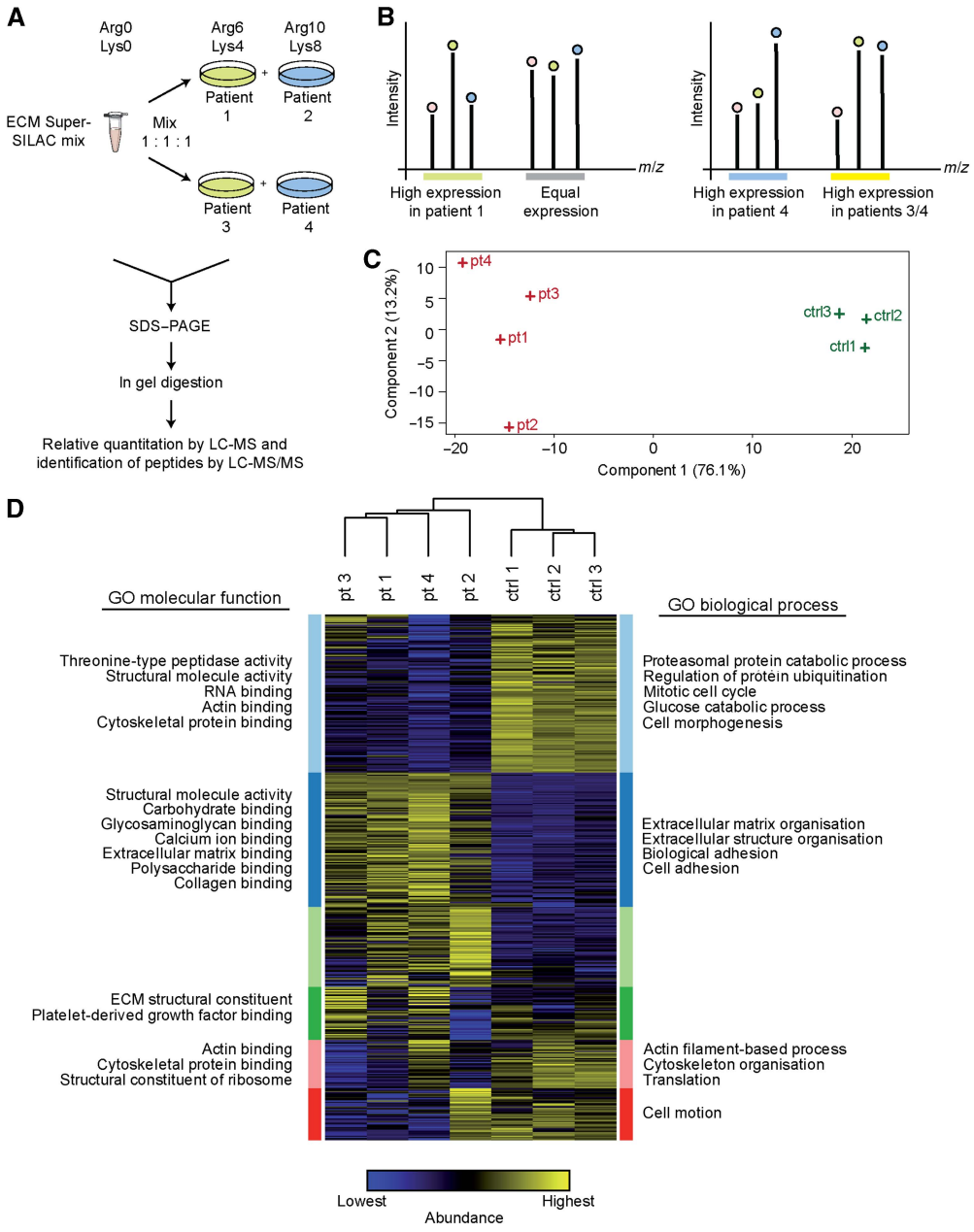

Figure 2 Analysis of quantitative differences in ECM compositions due to loss of C7. (**A**) Controls (light) were combined to a Super-SILAC mix to minimise differences in reference ECM isolations. These were spiked in 1:1:1 ratio to SILAC-labelled ECMs of RDEB fibroblasts (medium and heavy). The samples were processed as outlined and the resulting peptide mixtures were analysed by LC-MS/MS. (**B**) Peptide signal intensities recorded in MS spectra allowed relative quantification of RDEB and control ECM peptides, which were then combined to protein ratios. Coloured circles represent the respective SILAC state, as indicated in (A) (exemplified data). (**C**) Log2-transformed abundance changes of filtered ECM proteins were used for a principal component analysis. The two experimental groups are clearly separated, RDEB samples showing a bigger diversity in component 2. (**D**) Protein ratios were log2 transformed and z-score normalised. Columns containing data from the different samples were hierarchically clustered and rows containing protein entries were clustered by k-means. The proteins in k-means cluster were tested by DAVID (Huang da *et al*, 2009) for enrichment of GO CC and GO BP terms and selected terms are shown (full list in Supplementary Table S3; BH-adjusted *P*-value <0.01). Figures were produced using Servier Medical Art (www.servier.com).

performed a network analysis to assess the functional interactions of these extracellular proteins. This generated a protein interaction network consisting of 64 members (Figure 4). It became evident that basement membrane proteins were significantly less abundant in RDEB ($P<0.02$, BH adjusted), in particular, the laminin chains α4, β1, β2 and γ1, nidogen 1, collagen IV and several integrins. In contrast, interstitial collagens III, V and VI, protease inhibitors like serpins E1 and E2, and metalloproteases were more abundant ($P<0.008$, BH adjusted).

Altered abundance of PTMs of secreted proteins

We scanned secreted proteins for the presence of hydroxyproline and hydroxylysine residues, which are important for ECM

© 2013 EMBO and Macmillan Publishers Limited

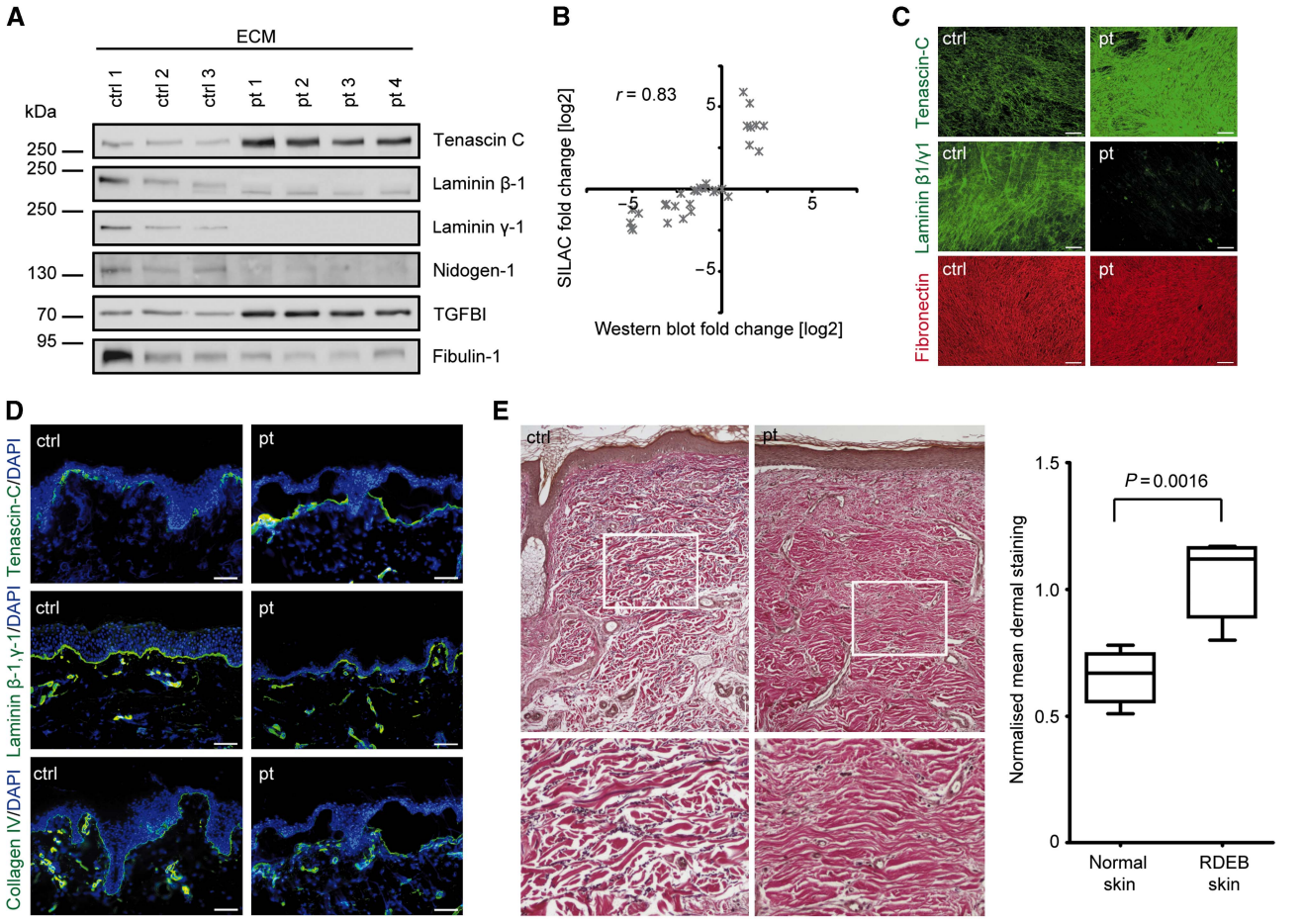

Figure 3 Altered deposition of ECM proteins in RDEB. (**A**) Purified ECM of control (ctrl) and RDEB (pt) fibroblasts were analysed by western blot using antibodies to proteins, which were indicated by MS-based proteomics to be significantly altered. Samples were normalised to cell number. (**B**) Correlation of western blot and SILAC ECM protein fold changes of RDEB versus control samples. (**C**) ECM of control (ctrl) and RDEB (pt) fibroblasts were stained using antibodies against annotated proteins, which were indicated by MS-based proteomics to be significantly altered. Fibronectin staining was used as a control for the ECM. (**D**) Immunofluorescence staining of control (ctrl) and RDEB (pt) skin in the skin of patient 3. (**E**) Fibrotic dermal ECM in RDEB. Normal skin (left panel): dermal ECM (red) with a loose, undulating fibrillar network, incorporating regular interconnected elastic fibres (black), vessels and adnex structures. RDEB skin (middle panel): tightly packed dermal ECM, fibre orientation parallel to the skin surface. Lower panels: magnification of detail (white frame in upper panels). Quantitation of normalised mean dermal staining intensity (right panel)—as a measure for fibrotic change—(normalisation to epidermal staining, y axis: relative units) shows a significant difference between normal and RDEB dermis ($P < 0.01$, two-tailed, unpaired *T*-test). Box-plot of results from skin specimens of RDEB patients and age- and localisation-matched healthy controls. $n = 5$. Scale bars represent 100 μm (C) and 50 μm (D).

stability and cross-linking (Monnier *et al*, 2005; Loenarz and Schofield, 2011), and analysed surrounding amino-acid motifs to gain further insights into potential mechanisms and biological functions of respective source proteins (Figure 5; Supplementary Figure S10). In total, 634 hydroxyproline and 130 hydroxylysine sites were identified (localisation score $\geqslant 0.75$, class I site, Andromeda score $\geqslant 100$) (Olsen *et al*, 2006). As expected, the largest groups of hydoxyproline and -lysine sites were variations of the collagen motifs Gly-X-Pro-OH and Gly-X-Lys-OH. However, also new hydroxylation motifs in other protein classes as defined by the matrisome project (Naba *et al*, 2012) were identified, especially in the case of proteins present in CM, of which many were glycoproteins, e.g., fibrillin-1 and -2 (Figure 5A and B; Supplementary Figure S10). Collagens detected in ECM and CM differed in their PTM status depending on the protein and not on the source compartment, suggesting that PTMs might have a role in protein-matrix integration and are dynamically modulated (Figure 5C; Supplementary Figure S10C). Interestingly, hydroxyproline sites identified in ECM and CM proteins in RDEB samples differed substantially from respective controls. Whereas sites detected in samples from patients 1, 3 and 4 were on average 2.3-fold less abundant than in controls, samples from patient 2 exhibited an even higher overall abundance level, however with differing contributions of single sites (Figure 5D; Supplementary Figure S10D; Supplementary Tables S5 and S6). Thus, loss of C7 in RDEB affects not only extracellular proteome composition but also the PTM status of secreted proteins.

Inactivation of metalloproteases

The protein interaction network shown in Figure 4 indicates high abundance of MMP2 and MMP14 and protease inhibitors, like TIMP3, in ECMs of RDEB skin fibroblasts. Increased

© 2013 EMBO and Macmillan Publishers Limited

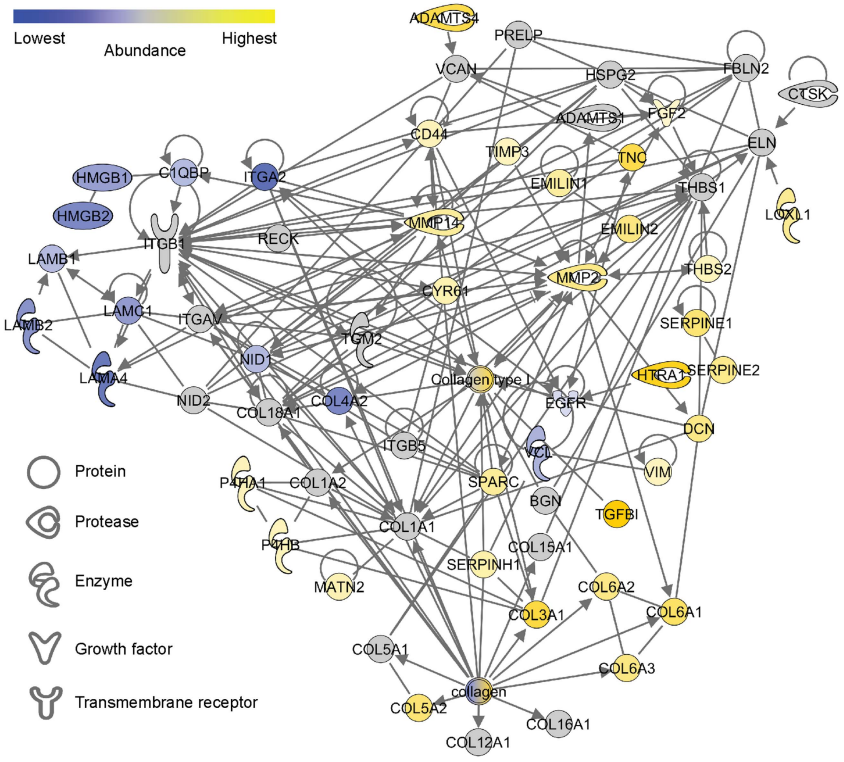

Figure 4 Network analysis reveals decrease in basement membrane proteins and increase in interstitial collagens. Network nodes represent quantified ECM proteins and edges known protein–protein interactions. Proteins with significantly lower abundance in RDEB than in controls are coloured blue and proteins with higher abundance yellow. Grey proteins show only significant changes in some of the patients. The network was generated by Path Designer, Ingenuity Systems.

abundance of both proteases in RDEB ECM was validated by western blot (Figure 6A). To estimate the proteolytic activity, control and RDEB fibroblasts were seeded on 3D collagen I gels and incubated for 3 days. During this period, control fibroblasts degraded the gel, whereas RDEB cells showed strongly reduced activity. Even after TNFα stimulation, which increases MMP14 expression and thereby MMP2 activation (Han *et al*, 2001), only little degradation of collagen I by RDEB fibroblasts was observed (Figure 6B). Protease inhibitor profiling linked the proteolytic activity to metalloproteases. In control cells, TAPI-O inhibited collagen I degradation, but neither leupeptin, nor the serine protease inhibitors SBTI and PMSF had an effect (Figure 6B). To specifically block the activity of membrane-bound metalloproteases, the furin inhibitor D-RVKR-CMK was included (Overall and Lopez-Otin, 2002). D-RVKR-CMK inhibited collagen I degradation by control cells, indicating that the proteolysis was due to MMP14 activity.

To test whether TIMP3, which can block MMP14 activity (Pavloff *et al*, 1992; Will *et al*, 1996) and accumulated in RDEB samples, was involved in MMP14 inactivation recombinant TIMP3 was also added to control cells and indeed blocked collagen I degradation (Figure 6B). On the other hand, the addition of RDEB CM, which contained soluble protease inhibitors, like TIMP1 and TIMP2, to control cells had no effect (Supplementary Figure S11).

The variation of MMP14 activity and abundance may also reflect differences in MMP14 recycling (Maquoi *et al*, 2003). To address the influence of lysosomal degradation of MMP14, cells were incubated with concanamycin A (ConA), an inhibitor of the lysosomal H^+-ATPase. In contrast to RDEB, ConA led to a pronounced accumulation of MMP14 in control cells (Figure 6C), which was reflected by an increase in MMP14 and MMP2 activity (Figure 6B and C), indicating impaired MMP14 turnover in RDEB.

To analyse proteolytic processing of membrane-bound MMP14, we fractionated two control and two RDEB ECMs by SDS–PAGE. The gel lanes were cut into pieces, ordered according to the molecular weight, in-gel digested by trypsin, and analysed by MS (Dix *et al*, 2008). In control samples, the MMP14 protein was almost entirely present in the full-length form (Figure 6D). In contrast, in RDEB samples, the full-length form represented only about half of the MMP14, and several smaller molecular weight forms were observed. Mapping of the peptides revealed that the smaller forms consisted only of the hemopexin-like domains 1–4, the transmembrane region and the cytoplasmic tail, i.e., had undergone shedding and lost the catalytic domain (Figure 6E). Thus, increased MMP14 shedding, increased abundance of inhibitors like TIMP3, and altered protein turnover contribute to diminished MMP14 activity in RDEB cells (Figure 6F).

Discussion

The ECM forms a complex meshwork around cells and organs, which does not act as a mere structural support but actively shapes the cellular microenvironment and has a vital part in

© 2013 EMBO and Macmillan Publishers Limited

intracellular signal initiation and transduction (Watt and Fujiwara, 2011). Here, we employed MS-based proteomics relying on SILAC labelling to investigate the protein microenvironment and the PTM status of secreted skin fibroblast proteins in health and disease. Several hundred proteins and their oxidative PTMs, which are important for structural stability, were quantified in ECM and CM samples of primary dermal fibroblasts.

Severe RDEB, associated with complete loss of C7, was chosen as a model disease to study the influence of a single protein on cellular microenvironment plasticity. Since the cellular microenvironment has a complex structure and

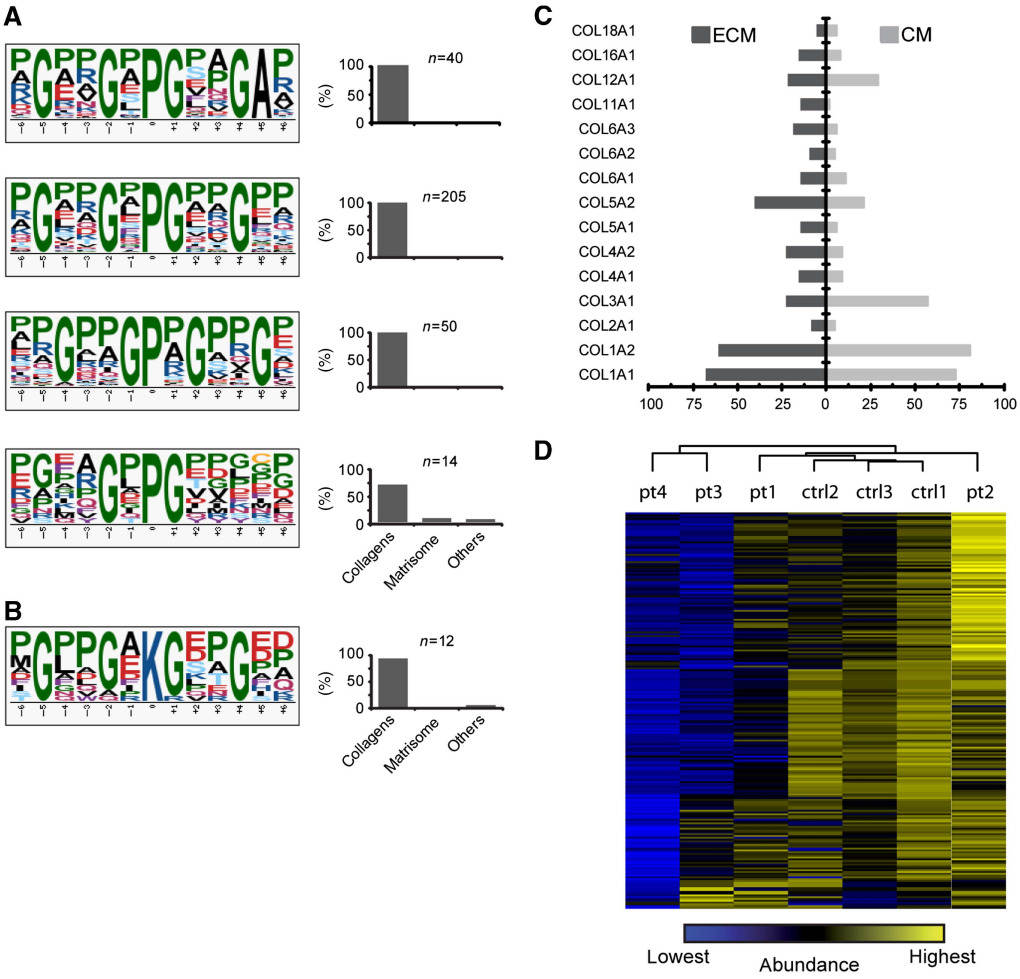

Figure 5 Alterations of oxidative PTMs. Hydroxyproline (**A**) and hydroxylysine (**B**) sites were scanned for sequence motifs using Motif-X (Schwartz *et al*, 2009; Chou and Schwartz, 2011). Site numbers and respective source proteins grouped according to the matrisome project (Naba *et al*, 2012) are shown as bar diagrams. (**C**) Numbers of hydroxyproline sites detected in collagens in ECM and CM, respectively, are indicated as bars. (**D**) Hydoxyproline sites ratios were normalised to respective source protein ratios (log2, z-transformed). Sites detected in RDEB and control ECMs are depicted as heatmap. Samples were hierarchically clustered and sites by k-means.

Figure 6 Decrease in protease activity in C7-deficient fibroblasts. (**A**) Western blot of MMP2 and MMP14 of ECM. (**B**) The blue rounds represent the intact collagen I matrix. Upon degradation of the matrix, the staining becomes white. In contrast to the RDEB cells (pt), control cells (ctrl) degrade the matrix, and the degradation is stimulated by the addition of TNFα. Inhibitor profiling demonstrates that the degradation is mediated by metalloproteases, since TAPIO, D-RVKR-CMK and TIMP3, but not serine and cystein protease inhibitors leupeptin, SBTI, and PSMF prevent it. ConA, inhibiting lysosomal degradation, leads only in control cells to enhanced degradation. (**C**) ConA leads to enhanced MMP2 activity in control cells as analysed by zymography. Western blot analysis reveals impaired MMP14 turnover in patient cells compared with control cells. Numbers indicating fold change as compared with untreated control. Samples were normalised to protein amount. (**D**) ECM proteins of RDEB (pt1, pt3) and control (ctrl2, ctrl3) cells were separated by SDS–PAGE and analysed by MS. The total number of detected MMP14 peptides in one sample was set to 100% and the distribution of peptides was mapped to respective gel slices. MMP14 appears to be shed in RDEB cells and not in control cells, as only $\sim$50% of the MMP14 peptides were detected in the 60-kDa gel slice harbouring full-length MMP14 in RDEB cells in contrast to almost 100% in control cells. (**E**) Schematic representation of the MMP14 molecule. Peptides derived from control cells (green) and RDEB cells (yellow) were mapped to the MMP14 molecule. Combined results of two biological replicates are shown. (**F**) Model of altered MMP14 turnover. Under healthy control conditions, C7 is present and active in the extracellular environment. MMP14 recycling and degradation is ensured to maintain degradation of collagen I and activation of MMP2. In RDEB, the ECM lacks C7, leading to an accumulation of MMP14, MMP2 and TIMP3. MMP14 and MMP2 activity is impaired due to the presence of inhibitors like TIMP3 and increased shedding of MMP14. Additionally, MMP14 recycling is perturbed further amplifying its accumulation.

© 2013 EMBO and Macmillan Publishers Limited

supramolecular organisation, it may not be adequately represented in analyses relying on gene expression arrays. Therefore, we took an unbiased proteomics approach to elucidate molecular disease mechanisms. Compared with a recent study using mRNA expression profiling, which detected upregulation of *COL5A1*, *COL12A1*, *ITGA3*, *ITGA6* and *TSP1* genes in RDEB (Ng *et al*, 2012), we identified substantially more deregulated extracellular proteins. Whereas mRNA abundances of the respective study correlated weakly with intracellular protein abundances of our samples, mRNA levels cannot be employed to deduce ECM protein abundances (Supplementary Figure S12). Hence, the proteomics

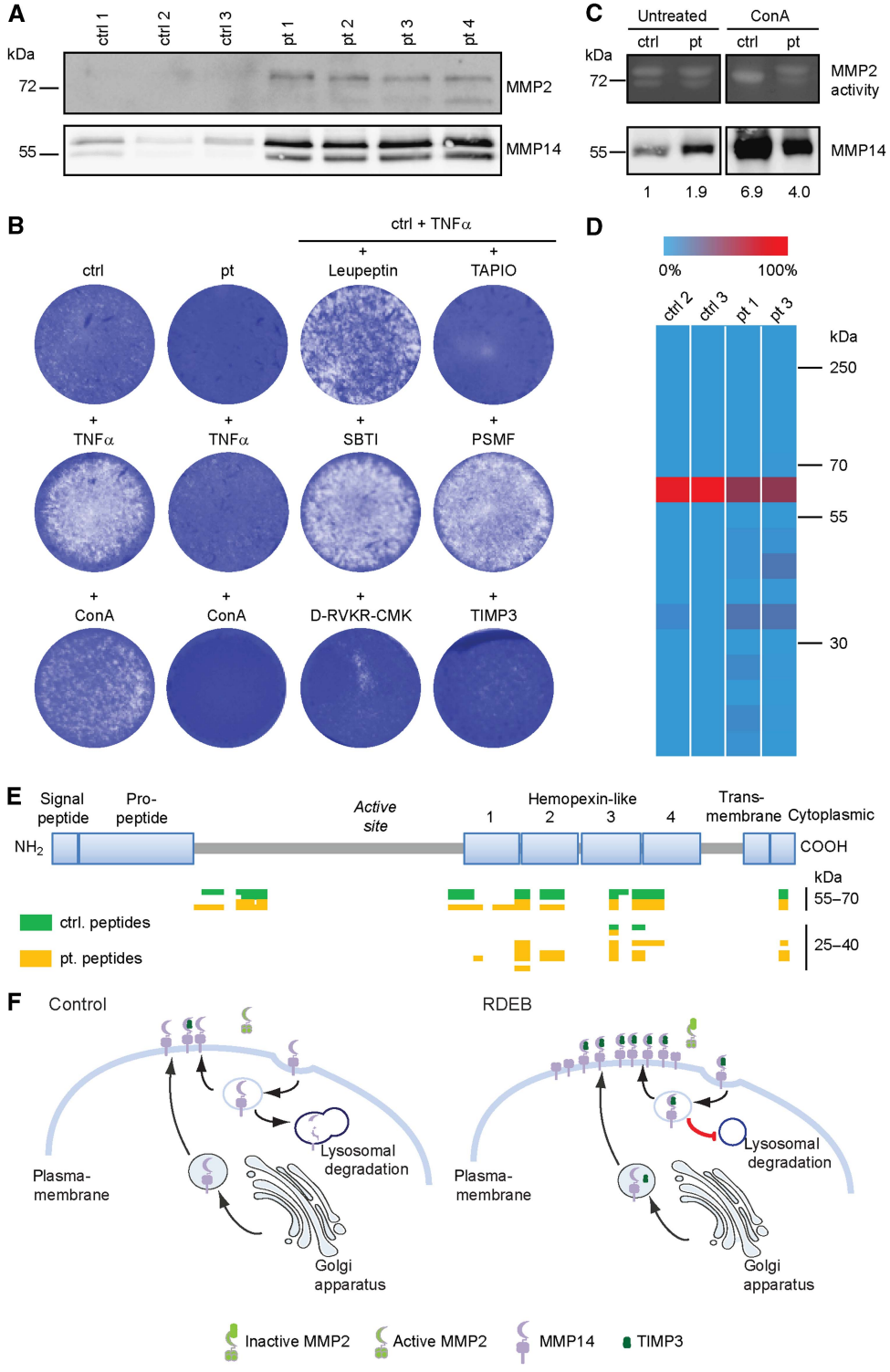

© 2013 EMBO and Macmillan Publishers Limited

experiments targeted directly the perturbed cellular microenvironment and generated data, which are not accessible by transcription analyses.

So far, only few studies have addressed the complexity of the skin fibroblast ECM proteome, often in a mostly qualitative manner. We have previously shown that SILAC labelling and cultivation of primary skin cells has only little influence on their proteomic composition (Sprenger *et al*, 2010) and we are confident that our cell culture system reflects the *in vivo* situation. In the present study, this was corroborated by the morphological analyses of normal and RDEB skin.

The high sensitivity of modern mass spectrometers led to detection of intracellular proteins despite careful purification of extracellular proteins before proteomic analysis. Therefore, a data processing pipeline was designed to filter extracellular proteins by bioinformatics means. As our main aim was the identification of pathological changes in the ECM proteome, we took a non-stringent approach and characterised in total 872 proteins as being extracellular based on their respective GO (39% carrying 'extracellular' GO terms), their repeated identification in biological replicates, and the presence of potential signal peptides. Twenty percent of the ECM proteins identified in this study were recently defined as components of the matrisome (Naba *et al*, 2012). This may not represent a final proof that all proteins in our tables are exclusively extracellular, but the definition of extracellular proteins is indeed not a trivial issue; new extracellular functions have been reported for classical intracellular proteins like glucose-6-phosphate isomerase, HSP90α and calreticulin (Butler and Overall, 2009).

We identified 764 oxidative PTM sites within the set of potential extracellular proteins. PTMs alter protein activity and stability, and great effort has been put into their mass spectrometric analysis. Enzymatic oxidations of ECM proteins are known to be essential for collagen stability, but hydroxylations have also been shown to alter signal transduction and protein–protein interactions (Loenarz and Schofield, 2011). New sequence motifs for hydoxyproline, which differ from the canonical collagen motifs and localise to other protein classes, could be characterised hinting at so far unstudied molecular functions. PTM abundances differed between RDEB and control samples, and it is very likely that the alterations exert direct effects on ECM stability and structure.

The disease proteomics approach uncovered new molecular players in skin fragility. Many of them have a logical link to the major clinical signs of severe RDEB, i.e., weak dermal-epidermal adhesion and dermal fibrosis, but the number and complexity of contributing molecules is much higher than anticipated. It became clear that lack of C7 does not simply represent a lost structural link, but causes a number of parallel changes on protein and PTM level, which influence the dermal-epidermal microenvironment.

Three novel aspects have clinical implications. First, the reduced abundance of basement membrane components is unexpected and intriguing. Relative deficiency of collagen IV, nidogen 1, or the laminin β1 and γ1 chains, which assemble to laminin 511, weakens the basement membrane suprastructure and amplifies the skin fragility caused by lack of functional anchoring fibrils. This is a pivotal finding that will influence the design of future molecular therapies.

Second, the inherently high production and secretion of ECM proteins in RDEB fibroblasts, including tenascin C, and interstitial collagens I, III, V and VI, clearly contribute to excessive scarring and dermal fibrosis in RDEB. Moreover, TGF-β, a growth factor that stimulates expression of many ECM proteins (Akhmetshina *et al*, 2012), was increased in the CM of RDEB fibroblasts. The combination of inherently elevated ECM synthesis and high secretion of TGF-β by RDEB fibroblasts is likely to be a major driver of scarring in RDEB skin, presumably further stimulated by other factors, such as inflammatory cytokines released through trauma-induced separation of the skin layers (Wynn and Ramalingam, 2012).

Third, the significant increase in proteases and protease inhibitors in RDEB ECM re-opens a field of investigation relating to molecular disease mechanisms. Skin fibroblasts express *MMPs 1, 2, 3, 9, 10, 13* and *14* (Loffek *et al*, 2011) and, in the past, investigators have suggested that increased MMP activity contributes to RDEB pathology (Winberg *et al*, 1989). The gene *MMP1* was the first one implicated in RDEB, before linkage analyses excluded its causative role (Colombi *et al*, 1992). In the present study, we found overrepresentation of MMP1 and MMP3 in CM of RDEB cells, and of MMP2 and MMP14 in the ECM. This was surprising, since increased proteolytic activity would apparently contrast with the accumulation of ECM in RDEB skin. The contradiction can be explained, at least in part, by the observation that although MMP14 protein abundance was increased, protease activity was significantly reduced in RDEB cells. *In vitro*, the RDEB cells mimicked the phenotype of *MMP14*-deficient mouse embryonic fibroblasts, i.e., both cells were unable to degrade collagen I gels (Holmbeck *et al*, 1999). In RDEB, decreased proteolysis could be caused by increased inhibition or processing of MMP14, by hampered turnover, or a combination of events. In support of the first prediction, increased levels of TIMP3 were identified in RDEB ECMs, and the addition of recombinant TIMP3 to control samples blocked collagen I degradation. In contrast, the addition of RDEB CM, which contained soluble protease inhibitors, to control cells had no effect rather pointing to a matrix-associated inhibitor like TIMP3 (Leco *et al*, 1994). The second prediction is supported by the fact that the ectodomain of MMP14 is shed in RDEB cells, rendering the membrane-bound stump inactive. In addition, MMP14 protein turnover was altered. Therefore, reduced MMP14 activity is a result of a combination of events.

Apart from the fact that the three points above will open new avenues of research into disease mechanisms in RDEB, a very exciting observation in this first disease proteomics study on RDEB was that the proteome profiles correlated with the severity of RDEB during disease progress. Specifically, ECM proteome alterations of patient 2, who developed the most severe RDEB phenotype in the course of the disease, were most different from those of the other patients. The clinical manifestations were intermediate in case of patients 1 and 3 and the respective ECM proteomes were most similar; the mildest clinical manifestations of the disease were observed in patient 4. These intriguing findings hold promise for future applications in personalised medicine, e.g., by developing prognostic markers based on the classification of protein abundances. Culture of skin fibroblasts is an easy and minimally invasive procedure, and quantitative proteomics

© 2013 EMBO and Macmillan Publishers Limited

is a powerful technique to identify cellular features, which are pertinent for both prognostication and development of targeted therapy approaches on an individual basis.

Taken together, the present study emphasises the potential of disease proteomics approaches to identify novel mechanisms of genetic diseases. The quantitative protein abundance information of extracellular proteins of healthy and pathologically altered cells provides a rich information source for the scientific community highlighting the complex changes in cellular microenvironment due to loss of a single protein, C7. The proteome alterations in RDEB serve as a starting point for discovery of hitherto unknown molecular mechanisms that not only explain the clinical phenotypic variation, but also identify targets for therapeutic intervention.

Materials and methods

Patients and RDEB diagnosis

Skin specimens were obtained from four newborns with skin blistering, but a negative family history for skin diseases. Immunofluorescence mapping revealed lack of C7 in the skin in all patients. Mutation analysis of the C7 gene, *COL7A1* (Kern *et al*, 2006, 2009) disclosed mutations leading to premature stop codons and thus confirmed the diagnosis (Table I). The clinical follow-up of the patients was during 2.5–10 years at the Epidermolysis Bullosa Center Freiburg. The study was approved by the Ethics Committee of Freiburg University and conducted according to the Declaration of Helsinki.

Cell culture and stable isotope labelling in cell culture

Primary dermal fibroblasts were isolated from the skin of the four patients and, as controls, from the foreskin of circumcised 3-, 4- and 9-year-old healthy boys (Sprenger *et al*, 2013). The cells were subcultured and passaged in SILAC–DMEM (Thermo Fisher, Langenselbold, Germany), supplemented with 10% dialysed FBS (Gibco, Invitrogen), 1% Antibiotic–Antimycotic (100×, Invitrogen), 1% L–glutamine (PAN Biotech), 42 mg/l L–arginine (Sigma–Aldrich), 73 mg/l L–lysine (Sigma–Aldrich) and 82 mg/l proline (Sigma–Aldrich) for the control population. RDEB fibroblasts were cultured and fully labelled for 2 weeks in the same way but through incorporation of either L-arginine-$^{13}C_6^{14}N_4$ and L-lysine-$^{2}H_4$ (Arg6, Lys4; Sigma-Aldrich) or L–arginine–$^{13}C_6$–$^{15}N_4$ and L-lysine-$^{13}C_6^{15}N_2$ (Arg10, Lys8; Sigma–Aldrich).

CM collection and ECM isolation

In all, 5×10^5 fully SILAC-labelled fibroblasts were seeded on 10 cm^2 cell culture dishes (BD, Heidelberg, Germany). One day later, the medium was changed and 50 μg/ml ascorbate (Sigma-Aldrich) was added to allow proper folding and secretion of collagens (Myllyharju and Kivirikko, 2004). Before harvesting the CM, the cells were washed 3× with PBS and starved for 14 h in serum-free medium to avoid interference of serum proteins with the MS analysis. CM was collected on day 4, centrifuged at 500 *g* 4°C for 10 min and filtered using 0.2 μm filters to remove cells and debris to prevent contamination by intracellular proteins. The CM of control and RDEB fibroblasts were mixed in a 1:1:1 ratio (the ratio was based on cell number) and concentrated by ultrafiltration using vivaspin columns with an mwco of 10 000 Da. Approximately 150 μg total protein (50 μg of each sample) was loaded on an SDS gel.

After 2 days in DMEM containing 50 μg/ml ascorbate and 10% FCS, the fibroblasts were washed three times with PBS. The cells were removed from the underlying ECM with 0.5% Triton X-100 in 20 mM NH_4OH for 30 s (Vlodavsky, 2001). The remaining ECM was then carefully washed 5× with PBS to eliminate intracellular contaminants. The ECM was solubilised with 4% SDS in 0.1 M Tris–HCl, pH 7.6 (Wisniewski *et al*, 2009). Aliquots of the different ECM isolations were mixed 1:1:1 (~50 μg for each sample) and prepared for MS analysis to determine the accurate mixing ratios. Based on this, whole ECM samples were mixed and concentrated using vivaspin columns with an mwco of 10 000 Da.

MS sample preparation

Samples were lysed in SDS–PAGE loading buffer, reduced with 1 mM DTT (Sigma–Aldrich) for 5 min at 95°C and alkylated using 5.5 mM iodoacetamide (Sigma–Aldrich) for 30 min at 25°C. Protein mixtures were separated by SDS–PAGE using 4–12% Bis–Tris mini gradient gels (NuPAGE, Invitrogen). The gel lanes were cut into 10 equal slices, which were in–gel digested with trypsin (Promega, Mannheim, Germany) (Shevchenko *et al*, 2006), and the resulting peptide mixtures were processed on STAGE tipps as described (Rappsilber *et al*, 2007). In case of the protomap approach, gel lanes were cut into 17 equal slices and processed as mentioned above (Dix *et al*, 2008).

Mass Spectrometry

Mass spectrometric measurements were performed on LTQ Orbitrap XL mass spectrometer (Thermo Fisher Scientific, Bremen, Germany) coupled to an Agilent 1200 nanoflow–HPLC (Agilent Technologies GmbH, Waldbronn, Germany). HPLC–column tips (fused silica) with 75 μm inner diameter (New Objective, Woburn, MA, USA) were self packed (Gruhler *et al*, 2005) with Reprosil–Pur 120 ODS–3 (Dr. Maisch, Ammerbuch, Germany) to a length of 20 cm. Samples were applied directly onto the column without pre–column. A gradient of A (0.5% acetic acid (high purity, LGC Promochem, Wesel, Germany) in water (HPLC gradient grade, Mallinckrodt Baker B.V., Deventer, The Netherlands) and B (0.5% acetic acid in 80% ACN (LC–MS grade, Wako, Germany) in water) with increasing organic proportion was used for peptide separation (loading of sample with 2% B; separation ramp: from 10–30% B within 80 min). The flow rate was 250 nl/min and for sample application 500 nl/min. The mass spectrometer was operated in the data–dependent mode and switched automatically between MS (max. of 1×10^6 ions) and MS/MS. Each MS scan was followed by a maximum of five MS/MS scans in the linear ion trap using normalised collision energy of 35% and a target value of 5000. Parent ions with a charge state from $z = 1$ and unassigned charge states were excluded for fragmentation. The mass range for MS was $m/z = 370$–2000. The resolution was set to 60 000. Mass–spectrometric parameters were as follows: spray voltage 2.3 kV; no sheath and auxiliary gas flow; ion–transfer tube temperature 125°C.

Identification of proteins and protein ratio assignment using MaxQuant

MS raw data files and respective information can be downloaded from the Peptide Atlas Data Repository (http://www.peptideatlas.org/PASS/PASS00080) (Desiere *et al*, 2006).

The MS raw data files were uploaded into the MaxQuant software version 1.2.0.18 (Cox and Mann, 2008), which performs peak detection, SILAC–pair detection, generates peak lists of mass error corrected peptides and database searches. A full-length IPI human database containing common contaminants such as keratins and enzymes used for in–gel digestion (based on IPI human version 3.68) was employed, carbamidomethylcysteine was set as fixed modification, oxidation of methionine, proline and lysine, and protein amino–terminal acetylation were set as variable modifications. Triple SILAC was chosen as quantitation mode. Three miss cleavages were allowed, enzyme specificity was trypsin/P + DP, and the MS/MS tolerance was set to 0.5 Da. The average mass precision of identified peptides was in general <1 p.p.m. after recalibration. Peptide lists were further used by MaxQuant to identify and relatively quantify proteins using the following parameters: peptide and protein FDRs, based on a forward-reverse database, were set to 0.01, maximum peptide posterior error probability (PEP) was set to 0.1, minimum peptide length was set to 6,

© 2013 EMBO and Macmillan Publishers Limited

minimum number peptides for identification and quantitation of proteins was set to two of which one must be unique, minimum ratio count was set to two, and identified proteins have been requantified. The 'match-between-run' option (2 min) was used. In case of the protomap approach, spectral counts were used as an estimate for relative protein quantification.

Data analysis

To obtain a list of potential secreted/extracellular proteins, the data were filtered using the freely available Perseus software (Cox *et al*, 2011) to extract proteins with the already annotated GO terms: extracellular region, extracellular space and ECM. Proteins that were present in the ECM fraction and CM were also included in the final protein lists, as well as proteins predicted by *in silico* analyses to carry a signal peptide (SignalP; default settings, www.cbs.dtu.dk/services/SignalP/) (Petersen *et al*, 2011). Subsequently, data were readjusted to a median of 1 and log2 transformed. DAVID 6.7 BETA (Huang da *et al*, 2009) was used to investigate protein enrichment in the ECM and CM fraction using functional annotation clustering with respective SP and PIR keywords with the default settings with a minimum significance of $P<0.01$.

The seven fibroblasts samples (pts and ctrls) were hierarchically clustered by the abundance of the identified proteins and the ratios for the individual proteins were k-means clustered to partition the proteins to six discrete clusters. To address the biological implications of the proteins in each cluster, Biological Process and Molecular Function GO terms were retrieved using DAVID (Huang da *et al*, 2009) and binomial probability test followed by Benjamini and Hochberg *P*-value adjustment was used to extract terms enriched in each cluster when tested against the remaining five clusters. A *P*-value after adjustment below 0.05 and at least five occurrences in the cluster were required to regard the enrichment as significant.

Received hydroxyproline and hydroxylysine sites were extracted for high confidence sites by requiring a MaxQuant localisation probability of >0.75 and an Andromeda Score of $\geqslant 100$ (Olsen *et al*, 2006; Cox *et al*, 2011). Pre-aligned peptides were further analysed by motif-x v1.2 10.05.06 (Schwartz and Gygi, 2005; Chou and Schwartz, 2011) with a central character of either K for hydroxylysine or P for hydroxyproline sites, a width of 13, a series of occurrences of 10 and a significance of 0.000001.

Western blot

Confluent cell cultures were extracted with 1% Nonidet P-40, 0.1 M NaCl, 0.025 M Tris/HCl, pH 7.4, containing Complete Protease Inhibitor Cocktail (Roche). The extracts were cleared from nuclei by centrifugation at 16 000 *g* for 10 min at 4°C, and the protein content of the extracts was determined by DC Protein Assay (Bio-Rad, München, Germany). An aliquot containing 50 μg of protein was separated on SDS–PAGE using a 7.5–12.5% gradient gel and transferred onto a nitrocellulose membrane. The membranes were blocked with 5% milk powder in 1 × TBS with 0.1% Tween-20 for a minimum of 1 h at room temperature and incubated for 1 h or overnight with one of the following antibodies: anti-nidogen (sc-33141), anti-fibulin-1 (sc-25281), anti-laminin β-1 (sc-5583), anti-laminin γ-1 (sc-17751), anti-actin (sc-47778) all from Santa Cruz Biotechnology; anti-Tenascin-C (MAB2138; R&D Systems, Wiesbaden, Germany), anti-MMP-14 (ab51074; Abcam), anti-ßig-h3 (D31B8; Cell Signaling Technology), or the collagen VII antibody NC2-10 (Bruckner-Tuderman *et al*, 1995). HRP-conjugated secondary antibodies and a chemiluminiscent detection assay (Immobilon Western, Millipore, Schwalbach, Germany) were used for visualisation according to manufacturer's instructions.

Immunofluorescence staining

For indirect immunofluorescence staining, fibroblasts grown on coverslips or skin cryosections were fixed with 4% PFA, or cold acetone and blocked with 2% BSA in PBS for 30 min at room temperature, followed by incubation with the primary antibody diluted in 0.2% BSA in PBS overnight at 4°C. After incubation with the secondary antibody in PBS for 1 h, the samples were embedded in fluorescence mounting medium (Dako, Hamburg, Germany). For staining of the ECM, 5×10^4 fibroblasts were grown on coverslips in DMEM containing 50 μg/ml ascorbate for 1 week. The cells were then removed as described above, and the ECM was fixed with 4% paraformaldehyde in PBS for 15 min and permeabilised with 0.1% Triton in PBS for 5 min at room temperature. After blocking for 30 min in 2% BSA in PBS, the ECM was incubated with the primary antibodies diluted in 1% BSA in PBS for 1 h. After incubation with the secondary antibody, the ECM was washed in PBS and embedded in fluorescence mounting medium (Dako). The following primary antibodies were used: anti-fibronectin (AB26245, AB2413; Abcam), anti-tenascin-C (MAB2138; R&D Systems), anti-ßig-h3 (D31B8; Cell Signaling Technology), anti-nidogen (sc-33141), anti-Laminin-β/γ1 (Progen, 10765), anti-ColIV (AB15633, Abcam) and the collagen VII LH7,2 (Bruckner-Tuderman *et al*, 1995). Alexa488- or Alexa594-conjugated secondary antibodies (Invitrogen) were used. Pictures were taken with an IF microscope (Zeiss Axio Imager; Zeiss, Oberkochen, Germany).

Staining of paraffin-embedded skin biopsy specimens

Skin specimens from the extremities of five RDEB patients (collagen VII negative, aged 25–45 at time of sampling) and five healthy controls (age and localisation matched) were Elastica van Gieson stained using standard methods. Mean dermal staining intensity in grey-scale pictures (16 bit) was measured with Image J (http://rsbweb.nih.gov/ij/) and normalised to mean epidermal staining. Two-tailed, unpaired T-test was used to calculate significance.

In situ collagen degradation assay and zymography

In all, 12-well culture plates were coated with a layer of neutralised rat tail collagen I (Gibco, Invitrogen) with a concentration of 300 μg/ml (1 ml/well) as described by the supplier and incubated for 2 h at 37°C to allow fibril formation. After washing with water and drying of the collagen gels, 5×10^4 fibroblasts were seeded onto the film. Five hours later, culture medium (DMEM, 10% FCS, 1% L-Glu, 1% penicillin/streptomycin) was added. The following day, culture medium was changed to serum-free DMEM and TNF-α, ConA or protease inhibitors were added. Following concentrations were used: 10 ng/ml TNF-α (Peprotech, Hamburg, Germany), 2 nM ConA (Peprotech), 25 μM TAPI-O (CalBiochem), 1 mM PMSF (Sigma-Aldrich), 1 μM SBTI (Sigma-Aldrich), 1 μg/ml Leupeptin (Sigma-Aldrich), 50 μM Furin Inhibitor I (Decanoyl-Arg-Val-Lys-Arg-CMK, Calbiochem/Merck, Darmstadt, Germany), 100 nM human recombinant TIMP3 (R&D Systems). After an incubation of 3 days in 37°C CM was harvested and the cells were removed by using 0.05% Trypsin and 0.02% EDTA in PBS (PAN Biotech, Aidenbach, Germany). The remaining collagen was visualised by Coomassie Brilliant Blue R-250 (Bio-Rad). Images were captured with an Image Quant™ LAS 4000 mini (GE Healthcare, Freiburg, Germany).

For MMP2 zymography, CM was centrifuged at 500 *g* at 4°C for 10 min and cells and cell debris of the remaining supernatant were removed by filtration using 0.2 μm filters. In all, 5 μg of proteins was separated on 10% ready gel gelatin zymogram gels (Bio-Rad) for 3 h at 100 V without prior reduction. Subsequently, the gel was washed 4 × in 2.5% Triton X-100 to remove SDS and incubated overnight in zymogram developing buffer (Bio-Rad) at 37°C to allow gelatin digestion. Gelatinase activity was visualised as colorless bands after staining the gel with Coomassie Brilliant Blue R-250.

siRNA-mediated silencing of collagen VII expression

For collagen VII knockdown, primary human dermal fibroblast were seeded at 30–50% confluence and transfected with siRNA duplexes specific to collagen VII the following day (Martins *et al*, 2009) or with irrelevant control siRNA duplexes (Eurogentec, Liège, Belgium) and

© 2013 EMBO and Macmillan Publishers Limited

Lipofectamine 2000 (Invitrogen) according to manufacturer's recommendations. Collagen VII expression was analysed by western blot.

Supplementary information

Supplementary information is available at the *Molecular Systems Biology* website (www.nature.com/msb).

Acknowledgements

This work was supported by the Excellence Initiative of the German Federal and State Governments through FRIAS-LifeNet and BIOSS, by grants SI 1281/2-1, BR 1475/12-1, and DE 1757/3-1 from the German Research Foundation, DFG, by the Network Epidermolysis bullosa (EB-Network) grant 01GM0830 from the German Ministry for Education and Research, BMBF, and by the Danish Natural Sciences Research Council. OS is supported by an Emmy-Noether grant of the DFG (SCHI 871/2-1) and a starting grant of the European Research Council (ERC-2011-StG 282111-ProteaSys). We thank C Has, M Boerries, A Heinz and C Cobzaru for helpful discussions; M. Zarei for maintenance of the MS; J Jackow and CW Franzke for kindly providing protease inhibitors; and M Schubert and K Thoma for excellent technical assistance.

Author contributions: LBT and JD managed and supervised the project. VK, CM, LBT and JD planned experiments. VK and CM performed experiments. VK, KTGR, JSK, OS, HB, and JD performed bioinformatics analyses and analysed data. VK, LBT, and JD wrote the paper with input from all authors.

Conflict of interest

The authors declare that they have no conflict of interest.

References

Akhmetshina A, Palumbo K, Dees C, Bergmann C, Venalis P, Zerr P, Horn A, Kireva T, Beyer C, Zwerina J, Schneider H, Sadowski A, Riener MO, MacDougald OA, Distler O, Schett G, Distler JH (2012) Activation of canonical Wnt signalling is required for TGF-beta-mediated fibrosis. *Nat Commun* **3:** 735

auf demKeller U, Prudova A, Eckhard U, Fingleton B, Overall CM (2013) Systems-level analysis of proteolytic events in increased vascular permeability and complement activation in skin inflammation. *Sci Signal* **6:** rs2

Boraldi F, Bini L, Liberatori S, Armini A, Pallini V, Tiozzo R, Ronchetti IP, Quaglino D (2003) Normal human dermal fibroblasts: proteomic analysis of cell layer and culture medium. *Electrophoresis* **24:** 1292–1310

Brizzi MF, Tarone G, Defilippi P (2012) Extracellular matrix, integrins, and growth factors as tailors of the stem cell niche. *Curr Opin Cell Biol* **24:** 645–651

Bruckner-Tuderman L, Nilssen O, Zimmermann DR, Dours-Zimmermann MT, Kalinke DU, Gedde-Dahl Jr T, Winberg JO (1995) Immunohistochemical and mutation analyses demonstrate that procollagen VII is processed to collagen VII through removal of the NC-2 domain. *J Cell Biol* **131:** 551–559

Butler GS, Overall CM (2009) Updated biological roles for matrix metalloproteinases and new 'intracellular' substrates revealed by degradomics. *Biochemistry* **48:** 10830–10845

Chou MF, Schwartz D (2011) Biological sequence motif discovery using motif-x. *Curr Protoc Bioinformatics* **Chapter 13:** Unit 13. 15–24

Colombi M, Gardella R, Zoppi N, Moro L, Marini D, Spurr NK, Barlati S (1992) Exclusion of stromelysin-1, stromelysin-2, interstitial collagenase and fibronectin genes as the mutant loci in a family with recessive epidermolysis bullosa dystrophica and a form of cerebellar ataxia. *Hum Genet* **89:** 503–507

Cox J, Mann M (2008) MaxQuant enables high peptide identification rates, individualized p.p.b.-range mass accuracies and proteome-wide protein quantification. *Nat Biotechnol* **26:** 1367–1372

Cox J, Neuhauser N, Michalski A, Scheltema RA, Olsen JV, Mann M (2011) Andromeda: a peptide search engine integrated into the MaxQuant environment. *J Proteome Res* **10:** 1794–1805

Del Galdo F, Shaw MA, Jimenez SA (2010) Proteomic analysis identification of a pattern of shared alterations in the secretome of dermal fibroblasts from systemic sclerosis and nephrogenic systemic fibrosis. *Am J Pathol* **177:** 1638–1646

Desiere F, Deutsch EW, King NL, Nesvizhskii AI, Mallick P, Eng J, Chen S, Eddes J, Loevenich SN, Aebersold R (2006) The PeptideAtlas project. *Nucleic Acids Res* **34:** D655–D658

Dix MM, Simon GM, Cravatt BF (2008) Global mapping of the topography and magnitude of proteolytic events in apoptosis. *Cell* **134:** 679–691

Engelke R, Becker AC, Dengjel J (2012) The degradative inventory of the cell: proteomic insights. *Antioxid Redox Signal* **17:** 803–812

Fine JD, Eady RA, Bauer EA, Bauer JW, Bruckner-Tuderman L, Heagerty A, Hintner H, Hovnanian A, Jonkman MF, Leigh I, McGrath JA, Mellerio JE, Murrell DF, Shimizu H, Uitto J, Vahlquist A, Woodley D, Zambruno G (2008) The classification of inherited epidermolysis bullosa (EB): Report of the Third International Consensus Meeting on Diagnosis and Classification of EB. *J Am Acad Dermatol* **58:** 931–950

Fritsch A, Loeckermann S, Kern JS, Braun A, Bosl MR, Bley TA, Schumann H, von Elverfeldt D, Paul D, Erlacher M, Berens von Rautenfeld D, Hausser I, Fassler R, Bruckner-Tuderman L (2008) A hypomorphic mouse model of dystrophic epidermolysis bullosa reveals mechanisms of disease and response to fibroblast therapy. *J Clin Invest* **118:** 1669–1679

Geiger T, Cox J, Ostasiewicz P, Wisniewski JR, Mann M (2010) Super-SILAC mix for quantitative proteomics of human tumor tissue. *Nat Methods* **7:** 383–385

Gruhler A, Olsen JV, Mohammed S, Mortensen P, Faergeman NJ, Mann M, Jensen ON (2005) Quantitative phosphoproteomics applied to the yeast pheromone signaling pathway. *Mol Cell Proteomics* **4:** 310–327

Hammami-Hauasli N, Schumann H, Raghunath M, Kilgus O, Luthi U, Luger T, Bruckner-Tuderman L (1998) Some, but not all, glycine substitution mutations in COL7A1 result in intracellular accumulation of collagen VII, loss of anchoring fibrils, and skin blistering. *J Biol Chem* **273:** 19228–19234

Han YP, Tuan TL, Wu H, Hughes M, Garner WL (2001) TNF-alpha stimulates activation of pro-MMP2 in human skin through NF-(kappa)B mediated induction of MT1-MMP. *J Cell Sci* **114:** 131–139

Has C, Bruckner-Tuderman L (2006) Molecular and diagnostic aspects of genetic skin fragility. *J Dermatol Sci* **44:** 129–144

Henningsen J, Rigbolt KT, Blagoev B, Pedersen BK, Kratchmarova I (2010) Dynamics of the skeletal muscle secretome during myoblast differentiation. *Mol Cell Proteomics* **9:** 2482–2496

Holmbeck K, Bianco P, Caterina J, Yamada S, Kromer M, Kuznetsov SA, Mankani M, Robey PG, Poole AR, Pidoux I, Ward JM, Birkedal-Hansen H (1999) MT1-MMP-deficient mice develop dwarfism, osteopenia, arthritis, and connective tissue disease due to inadequate collagen turnover. *Cell* **99:** 81–92

Huang da W, Sherman BT, Lempicki RA (2009) Systematic and integrative analysis of large gene lists using DAVID bioinformatics resources. *Nat Protoc* **4:** 44–57

Kern JS, Gruninger G, Imsak R, Muller ML, Schumann H, Kiritsi D, Emmert S, Borozdin W, Kohlhase J, Bruckner-Tuderman L, Has C (2009) Forty-two novel COL7A1 mutations and the role of a frequent single nucleotide polymorphism in the MMP1 promoter in modulation of disease severity in a large European dystrophic epidermolysis bullosa cohort. *Br J Dermatol* **161:** 1089–1097

Kern JS, Kohlhase J, Bruckner-Tuderman L, Has C (2006) Expanding the COL7A1 mutation database: novel and recurrent mutations and unusual genotype-phenotype constellations in 41 patients with dystrophic epidermolysis bullosa. *J Invest Dermatol* **126:** 1006–1012

© 2013 EMBO and Macmillan Publishers Limited

Leco KJ, Khokha R, Pavloff N, Hawkes SP, Edwards DR (1994) Tissue inhibitor of metalloproteinases-3 (TIMP-3) is an extracellular matrix-associated protein with a distinctive pattern of expression in mouse cells and tissues. *J Biol Chem* **269:** 9352–9360

Loenarz C, Schofield CJ (2011) Physiological and biochemical aspects of hydroxylations and demethylations catalyzed by human 2-oxoglutarate oxygenases. *Trends Biochem Sci* **36:** 7–18

Loffek S, Schilling O, Franzke CW (2011) Series 'matrix metalloproteinases in lung health and disease': Biological role of matrix metalloproteinases: a critical balance. *Eur Respir J* **38:** 191–208

Maquoi E, Peyrollier K, Noel A, Foidart JM, Frankenne F (2003) Regulation of membrane-type 1 matrix metalloproteinase activity by vacuolar H + -ATPases. *Biochem J* **373:** 19–24

Martins VL, Vyas JJ, Chen M, Purdie K, Mein CA, South AP, Storey A, McGrath JA, O'Toole EA (2009) Increased invasive behaviour in cutaneous squamous cell carcinoma with loss of basement-membrane type VII collagen. *J Cell Sci* **122:** 1788–1799

Monnier VM, Mustata GT, Biemel KL, Reihl O, Lederer MO, Zhenyu D, Sell DR (2005) Cross-linking of the extracellular matrix by the maillard reaction in aging and diabetes: an update on 'a puzzle nearing resolution'. *Ann NY Acad Sci* **1043:** 533–544

Myllyharju J, Kivirikko KI (2004) Collagens, modifying enzymes and their mutations in humans, flies and worms. *Trends Genet* **20:** 33–43

Naba A, Clauser KR, Hoersch S, Liu H, Carr SA, Hynes RO (2012) The matrisome: in silico definition and *in vivo* characterization by proteomics of normal and tumor extracellular matrices. *Mol Cell Proteomics* **11:** M111.014647

Ng YZ, Pourreyron C, Salas-Alanis JC, Dayal JH, Cepeda-Valdes R, Yan W, Wright S, Chen M, Fine JD, Hogg FJ, McGrath JA, Murrell DF, Leigh IM, Lane EB, South AP (2012) Fibroblast-derived dermal matrix drives development of aggressive cutaneous squamous cell carcinoma in patients with recessive dystrophic epidermolysis bullosa. *Cancer Res* **72:** 3522–3534

Olsen JV, Blagoev B, Gnad F, Macek B, Kumar C, Mortensen P, Mann M (2006) Global, *in vivo*, and site-specific phosphorylation dynamics in signaling networks. *Cell* **127:** 635–648

Ong SE, Blagoev B, Kratchmarova I, Kristensen DB, Steen H, Pandey A, Mann M (2002) Stable isotope labeling by amino acids in cell culture, SILAC, as a simple and accurate approach to expression proteomics. *Mol Cell Proteomics* **1:** 376–386

Overall CM, Lopez-Otin C (2002) Strategies for MMP inhibition in cancer: innovations for the post-trial era. *Nat Rev Cancer* **2:** 657–672

Pavloff N, Staskus PW, Kishnani NS, Hawkes SP (1992) A new inhibitor of metalloproteinases from chicken: ChIMP-3. A third member of the TIMP family. *J Biol Chem* **267:** 17321–17326

Petersen TN, Brunak S, von Heijne G, Nielsen H (2011) SignalP 4.0: discriminating signal peptides from transmembrane regions. *Nat Methods* **8:** 785–786

Pflieger D, Chabane S, Gaillard O, Bernard BA, Ducoroy P, Rossier J, Vinh J (2006) Comparative proteomic analysis of extracellular matrix proteins secreted by two types of skin fibroblasts. *Proteomics* **6:** 5868–5879

Rappsilber J, Mann M, Ishihama Y (2007) Protocol for micro-purification, enrichment, pre-fractionation and storage of peptides for proteomics using StageTips. *Nat Protoc* **2:** 1896–1906

Schwartz D, Chou MF, Church GM (2009) Predicting protein post-translational modifications using meta-analysis of proteome scale data sets. *Mol Cell Proteomics* **8:** 365–379

Schwartz D, Gygi SP (2005) An iterative statistical approach to the identification of protein phosphorylation motifs from large-scale data sets. *Nat Biotechnol* **23:** 1391–1398

Shevchenko A, Tomas H, Havlis J, Olsen JV, Mann M (2006) In-gel digestion for mass spectrometric characterization of proteins and proteomes. *Nat Protoc* **1:** 2856–2860

Smyth GK (2004) Linear models and empirical bayes methods for assessing differential expression in microarray experiments. *Stat Appl Genet Mol Biol* **3:** Article 3

Sprenger A, Kuttner V, Biniossek ML, Gretzmeier C, Boerries M, Mack C, Has C, Bruckner-Tuderman L, Dengjel J (2010) Comparative quantitation of proteome alterations induced by aging or immortalization in primary human fibroblasts and keratinocytes for clinical applications. *Mol Biosyst* **6:** 1579–1582

Sprenger A, Kuttner V, Bruckner-Tuderman L, Dengjel J (2013) Global proteome analyses of SILAC-labeled skin cells. *Methods Mol Biol* **961:** 179–191

Titeux M, Pendaries V, Tonasso L, Decha A, Bodemer C, Hovnanian A (2008) A frequent functional SNP in the MMP1 promoter is associated with higher disease severity in recessive dystrophic epidermolysis bullosa. *Hum Mutat* **29:** 267–276

Todorovic V, Desai BV, Eigenheer RA, Yin T, Amargo EV, Mrksich M, Green KJ, Patterson MJ (2010) Detection of differentially expressed basal cell proteins by mass spectrometry. *Mol Cell Proteomics* **9:** 351–361

van den Akker PC, Jonkman MF, Rengaw T, Bruckner-Tuderman L, Has C, Bauer JW, Klausegger A, Zambruno G, Castiglia D, Mellerio JE, McGrath JA, van Essen AJ, Hofstra RM, Swertz MA (2011) The international dystrophic epidermolysis bullosa patient registry: an online database of dystrophic epidermolysis bullosa patients and their COL7A1 mutations. *Hum Mutat* **32:** 1100–1107

Vlodavsky I (2001) Preparation of extracellular matrices produced by cultured corneal endothelial and PF-HR9 endodermal cells. *Curr Protoc Cell Biol* **Chapter 10:** Unit 10.4

Waterman EA, Sakai N, Nguyen NT, Horst BA, Veitch DP, Dey CN, Ortiz-Urda S, Khavari PA, Marinkovich MP (2007) A laminin-collagen complex drives human epidermal carcinogenesis through phosphoinositol-3-kinase activation. *Cancer Res* **67:** 4264–4270

Watt FM, Fujiwara H (2011) Cell-extracellular matrix interactions in normal and diseased skin. *Cold Spring Harb Perspect Biol* **3**(pii)**:** a005124

Will H, Atkinson SJ, Butler GS, Smith B, Murphy G (1996) The soluble catalytic domain of membrane type 1 matrix metalloproteinase cleaves the propeptide of progelatinase A and initiates autoproteolytic activation. Regulation by TIMP-2 and TIMP-3. *J Biol Chem* **271:** 17119–17123

Winberg JO, Gedde-Dahl Jr. T, Bauer EA (1989) Collagenase expression in skin fibroblasts from families with recessive dystrophic epidermolysis bullosa. *J Invest Dermatol* **92:** 82–85

Wisniewski JR, Zougman A, Nagaraj N, Mann M (2009) Universal sample preparation method for proteome analysis. *Nat Methods* **6:** 359–362

Wynn TA, Ramalingam TR (2012) Mechanisms of fibrosis: therapeutic translation for fibrotic disease. *Nat Med* **18:** 1028–1040

Zimmermann AC, Zarei M, Eiselein S, Dengjel J (2010) Quantitative proteomics for the analysis of spatio-temporal protein dynamics during autophagy. *Autophagy* **6:** 1009–1016

***Molecular Systems Biology* is an open-access journal published by the *European Molecular Biology Organization* and *Nature Publishing Group*. This work is licensed under a Creative Commons Attribution-Noncommercial-No Derivative Works 3.0 Unported Licence. To view a copy of this licence visit http://creativecommons.org/licenses/by-nc-nd/3.0/.**

© 2013 EMBO and Macmillan Publishers Limited